ChemPubSoc Europe

DOI: 10.1002/cssc.201800027

CHEMSUSCHEM Full Papers

Kinetics-Controlled Degradation Reactions at Crystalline LiPON/Li_xCoO_2 and Crystalline LiPON/Li-Metal Interfaces

Kevin Leung,*[a] Alexander J. Pearse,[b] A. Alec Talin,[c] Elliot J. Fuller,[c] Gary W. Rubloff,[b] and Normand A. Modine[a]

Detailed understanding of solid–solid interface structure–function relationships is critical for the improvement and wide deployment of all-solid-state batteries. The interfaces between lithium phosphorous oxynitride (LiPON) solid electrolyte material and lithium metal anode, and between LiPON and Li_xCoO_2 cathode, have been reported to generate solid–electrolyte interphase (SEI)-like products and/or disordered regions. Using electronic structure calculations and crystalline LiPON models, we predict that LiPON models with purely P–N–P backbones are kinetically inert towards lithium at room temperature. In contrast, transfer of oxygen atoms from low-energy Li_xCoO_2(104) surfaces to LiPON is much faster under ambient conditions. The mechanisms of the primary reaction steps, LiPON structural motifs that readily reacts with lithium metal, experimental results on amorphous LiPON to partially corroborate these predictions, and possible mitigation strategies to reduce degradations are discussed. LiPON interfaces are found to be useful case studies for highlighting the importance of kinetics-controlled processes during battery assembly at moderate processing temperatures.

Introduction

The deployment of solid electrolytes in all-solid-state batteries in transportation energy storage applications can effectively address safety concerns associated with current commercial, organic-solvent-based lithium-ion batteries. Technical issues remain,[1–6] many of which are associated with buried solid-solid interfaces between electrolytes and electrodes.[7] Although cross-sectional transmission electron microscopy (TEM),[8–10] potential mapping,[11,12] X-ray photoemission spectroscopy,[13–17] and other experimental techniques have provided a wealth of information about such interfaces, so far they lack sufficient resolution to yield atomic length-scale details—especially in materials without crystalline order.

Electronic structure (e.g., density functional theory, DFT) calculations on model solid–solid interfaces yield insights that are complementary to measurements.[18–26] They can further raise novel scientific questions that will attract experimental inquiry. One important topic to address is the charge separation associated with the solid-state electric double layer (EDL) at such interfaces.[27] Electric fields associated with the EDL are expected to aid Li^+ diffusion during charge and discharge events, but may also accelerate interfacial chemical or electrochemical reactions between the electrode and electrolyte to form a "solid–electrolyte interphase" (SEI).[28] Such SEI products have indeed been reported at some all-solid battery interfaces. Liquid electrolytes also take part in interfacial reactions, although in that case the SEI is often formed during the first few charging cycles, whereas in all-solid-state batteries part of the SEI already emerges during battery assembly.[29]

This work focuses on crystalline model of lithium phosphorous oxynitride ("LiPON")[8,13,15,17,30–43] solid electrolyte materials in contact with the lithium metal [Li(s)] anode and lithium cobalt oxide (Li_xCoO_2) cathode surfaces. LiPON interfaces present interesting case studies. It has been reported that LiPON forms interfacial reaction products when in contact with Li(s)[15] and with Li_xCoO_2,[8–10,13,17] especially at elevated temperature, although the batteries continue to function. Heating may even reduce interfacial charge transfer resistance.[44] Therefore modeling of the electrode/electrolyte interfaces, which control the EDL and charge transfer, necessarily requires first addressing the reactions that produce SEI. Herein we distinguish SEI products obtained from gaseous precursors during battery fabrication and assembly, before the solid component being grown is fully formed, and SEI products that emerge during cycling.[29] The latter register as an increase in SEI after cycling, and are the focus of our modeling work.

We applied DFT calculations to study LiPON interfacial reactions on the low energy Li(001) and Li_xCoO_2(104) surfaces. While many solid-state batteries feature silicon anodes,[33] the top layer of lithiated silicon is typically terminated by Li

[a] Dr. K. Leung, Dr. N. A. Modine
Sandia National Laboratories, MS 1415
Albuquerque, NM 87185 (USA)
E-mail: kleung@sandia.gov

[b] Dr. A. J. Pearse, Prof. G. W. Rubloff
Department of Materials Science and Engineering,
University of Maryland, College Park, Maryland 20740 (USA)

[c] Dr. A. A. Talin, Dr. E. J. Fuller
Sandia National Laboratories, MS 9161
Livermore, CA 94550 (USA)

Supporting Information and the ORCID identification number(s) for the author(s) of this article can be found under: https://doi.org/10.1002/cssc.201800027.

This publication is part of a Special Issue on Interfacing Theory and Experiment for the Development of Energy Materials.
Please visit the issue at http://doi.org/10.1002/cssc.v11.12.

atoms,[45] which minimizes the surface energy. Therefore our work may also be relevant to Si anodes. On the cathode side, our calculations draw on previous modeling work on Li_xCoO_2 bulk crystal,[46] its (vacuum) surfaces,[46–48] electron spin distributions,[8,23] and on LiPON studies using model structures.[26,49–53] Related modeling work on Li(Mn,Ni,Co)O_2 surfaces are also relevant.[54,55] Our work also benefits from single-phase thermodynamics predictions,[56] which describe the stability window outside which LiPON and electrode materials can react. If reactions are not limited by slow kinetics and reach equilibrium, single-phase thermodynamics efficiently predict the final, most stable interfacial products. However, unlike crystal growth associated with cathode synthesis routinely conducted at 700–1000 °C, the processing temperatures for fabricating interfaces are much lower (150–300 °C for oxides, and lower for sulfides). Therefore, metastable products may dominate at solid-solid interfaces. Indeed, there is experimental evidence that kinetics- rather than thermodynamics-determined products are formed in some all-solid batteries.[8,57] Even more obvious examples are the anode SEI in organic liquid electrolyte-based batteries. The SEI films there are formed at room temperature; many SEI components are demonstrably metastable and exist only because of complex kinetics constraints.[58] In liquid-electrolyte SEI, single-phase thermodynamics predictions clearly fail; combining kinetics and thermodynamics modeling is crucial to yield insights that can be related to measurements.

In this study, we apply perspectives from liquid-state batteries[58–60] and examine the activation energies of rate-limiting primary degradation reactions at explicit electrode/electrolyte interfaces. A few subsequent, secondary reactions are also considered; in some cases, they are faster than the first reactions which activate the chain of degradation events. Unlike single-phase thermodynamic calculations,[56] this kinetic approach does not predict the final products, which may be the culmination of reactions many steps later. Instead, we examine the temperature and voltage dependence of primary reaction steps, elucidate the mechanisms, and gain insight into what material variations can raise reaction barriers. This will allow mitigation of degradation processes. We predict faster degradation reactions on the cathode than on the anode surface, but some reactions can occur at room temperature at both interfaces.

For experimental work, we perform conductivity measurements on pristine and LiPON-coated Li_xCoO_2 to support the prediction that transfer of chemical species between the LiPON surface layers and Li_xCoO_2 occurs. Finally, X-ray photoelectron spectroscopy (XPS) is used to confirm chemical changes at the cathode/LiPON interface.

There are many challenges associated with the computational approach stated above. LiPON encompasses a family of amorphous materials synthesized with different deposition techniques. Different LiPON materials exhibit variations in chain length and stoichiometry, especially in the nitrogen content. We start with a crystalline Li_2PO_2N model[49] which is close to the stoichiometry obtained in atomic layer deposition (ALD) synthesis.[33] The model has infinitely long chains, exclusively 2-coordinated N atoms, and no P–O–P or $N(P)_3$ motif in the backbone, although the latter are minority LiPON features under low-temperature growth conditions.[13,14,34] We also consider defected LiPON modified from perfect LiPON crystals. We stress that our modeling work is not meant to match any particular set of measurements. Instead, we elucidate interfacial reaction mechanisms and kinetically stable/reactive structure motifs that should be of general interest, and inform interpretations about the reactions of different LiPON realizations.

Atomic structures normally used as the starting points for modeling efforts are largely unknown from existing measurements of buried battery interfaces. Registry and lattice matching between two solid-state components are nontrivial; the need to account for possible addition or removal of Li atoms at battery interfaces adds complexity. As interfaces usually involve spatial heterogeneities, the predicted reaction rates may span a continuum. Therefore multiple reactive sites are examined. The Co charge and spin states at the LiPON interface can change with the coordination environment. The reproducibility of the predicted set of Li_xCoO_2 spin states is an issue. Previous studies have mostly focused on either $x=0$ or $x=1$ surfaces,[46–48] which exhibit all Co^{3+} or Co^{4+}, circumventing this issue. We show that the problem must be confronted for slab geometries at intermediate x values. Regarding voltage dependence,[28,61–64] reactions at interfaces may or may not vary with applied potential, depending on whether the rate-limiting step involves electron transfer or not; this distinction will be examined. Qualitative comparison between our predictions and reported experimental results is presented in the Discussion section.

Results

LiPON/lithium interfaces

LiPON slab on Li(s) surface

Reactions between LiPON and lithium metal to form Li_3P, Li_2O, and $LiPN_2$ are thermodynamically favorable,[56] indicating that LiPON is metastable against lithium. It is the reaction rate that needs to be determined. Figure 1a depicts a simulation cell with model LiPON in a slab geometry. There are 18 LiPON O atoms in contact with the Li metal. One Li atom is inserted beneath each O^{2-} to form an interlayer (see the Supporting Information). Figure 1c and d show expanded views of the reaction region before and after breaking one P–O bond, respectively. After optimizing the atomic configuration, the detached O^{2-} anion becomes buried inside the Li metal, coordinated to 6 Li with O–Li bond lengths of 2.1 Å or less (Figure 1d). Bader charge analysis[65] is qualitatively consistent with the transfer of two electron from Li metal to the original P^{5+} to form P^{3+} with a broken bond. The energy released is significant, with $\Delta E = -0.63$ eV.

At the transition state, the P–O distance is 2.27 Å. The reaction barrier ΔE^* is predicted to be a very substantial 2.15 eV. By using an Arrhenius rate expression $1/\tau(T) = k \exp(-\Delta G^*/k_BT)$, approximating the free energy barrier with the zero temperature ΔE^* and assuming a kinetic prefactor of $k = 10^{12}\,s^{-1}$, the room-temperature reaction time $\tau(T)$ associated with

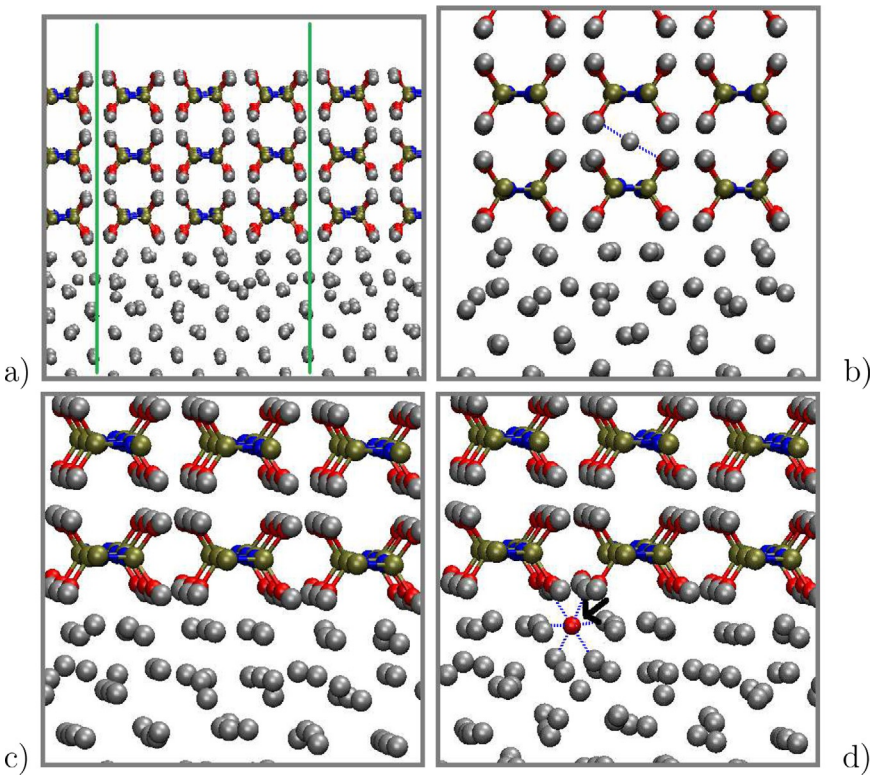

Figure 1. a) Periodically replicated simulation cell (green boundaries) containing LiPON slab on Li metal. A vacuum region exists. b) Expanded view with an extra Li atom in LiPON interior region. c, d) Interface region in (a) expanded, before and after P–O bond-breaking, respectively. Silver, red, blue, and dark green represent Li, O, N, and P atoms, respectively. Blue dashed lines indicate selected Li–O distances that are less than 2.2 Å. Black arrows in some panels indicate the motion of key atoms in bond-breaking reactions.

breaking a bond with $\Delta E^* = 0.92$ eV is about an hour; breaking a bond with $\Delta E^* > 1.1$ eV takes far longer than battery operational time scales. At $T \approx 690$ K, $\tau(T)$ shrinks to one hour. However, this is above the lithium metal melting point. Lithium interfaces must be assembled below 500 K. At this temperature, the predicted ΔE^* is too still high for the reaction to occur within reasonable timescales. The high activation energy associated with P–O bond cleavage is likely the reason that Li_3PO_4 has also been used in coating layers for lithium metal[66] even though Li_3PO_4 is also thermodynamically unstable agains Li metal.[53]

We have also attempted to break the other 17 P–O bonds at the interface. The ΔE predicted depends on the coordination of the released O^{2-}, and ranges from -0.77 to -0.30 eV with an average of -0.53 ± 0.03 eV. ΔE^* calculations are more costly and are only attempted for two other P–O cleavage events. $\Delta E^* = 2.16$ and 2.30 eV are found to be associated with breaking these other bonds, again indicating that the reaction would be very slow under ambient conditions.

Attempts to break single P–N bonds in a LiPON chain at the interface and then re-optimize the configuration lead to either reformation of the P–N bond and the original LiPON structure, or a metastable structure with the P and N atoms separated by 2.22 Å (not shown) instead of the 1.55–1.59 Å P–N bond length in equilibrium LiPON models. The energy of the configuration with a broken bond is a very significant 1.76 eV above that of the intact LiPON slab. Although breaking two P–N bonds and depositing the N atom onto the Li metal far from the two P atoms is exothermic, we do not find a pathway with a sufficiently low reaction barrier to justify this mechanism at room temperature. Thus we conclude that neither P–O nor P–N cleavage is kinetically viable at the crystalline LiPON/Li metal interface.

Because the model system is metallic and the simulation cell has a vacuum region, the instantaneous electrochemical potential or voltage V_e of this system can be unambiguously assigned. V_e is the work function Φ divided by $|e|$ and subtracted by 1.37 V.[28] Before breaking the P–O bond, $V_e = 0.12$ V vs. $Li^+/Li(s)$ reference. The orbital alignment is depicted in Figure 2a. Unlike the calculations in Refs. [52, 53], Figure 2a accounts for explicit LiPON/lithium anode interfaces; although this figure represents thin films, absolute (not relative) orbital energy levels can be obtained.

V_e is sufficiently close to the equilibrium voltage below which Li metal is stable, at 0.0 V vs. $Li^+/Li(s)$, that the predicted ΔE and ΔE^* can be regarded as associated with approximately the equilibrium Li-plating or stripping voltage. If P–O bond breaking in Figure 1d is an electrochemical reaction, according to the Butler–Volmer equation,[67] ΔE^* is expected to be lowered by 0.12 eV relative to the same reaction at 0.0 V, assuming that the rate-determining step involves two-electron transfer and $\alpha = 0.5$.[67] This reduction in ΔE^* would not change the conclusion that ΔE^* remains far too high for P–O or P–N cleavage to occur at room temperature. We will show below that, in

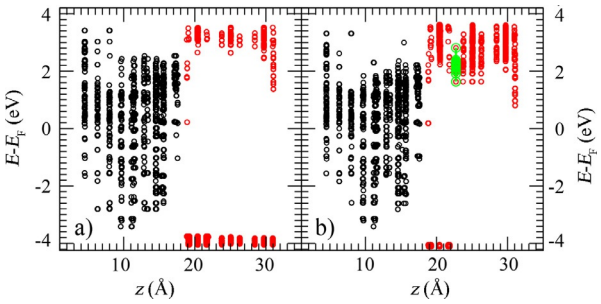

Figure 2. a, b) Kohn–Sham orbitals corresponding to Figure 1 a and b, respectively. Black and red circles represent location of orbitals along *z* axis (perpendicular to interface) localized on Li metal and LiPON atoms, respectively. Green circles represent orbitals on the excess Li added in the LiPON interior region. They lie above the Fermi level (E_F) and are unoccupied.

fact, barriers associated with LiPON reactions on lithium metal do not strongly depend on V_e.

It is also of interest to ascertain whether long-range electron injection into defects in the middle of the LiPON solid region can occur. In batteries based on liquid electrolytes, such e^- transfer has been widely acknowledged. To this end, we have attempted to break a P–N bond in the LiPON crystal region away from the interface, with one or two Li inserted in the void space around the broken bond, while maintaining charge neutrality. Such a "grand canonical" scheme represents reactions accompanied by excess Li migration into LiPON from Li metal. After optimization of the atomic configuration, the P–N bond is reconstituted (Figure 1 b) and Bader charge analysis indicates negligible excess e^- in the Li inserted. This finding is consistent with the predicted orbital alignment (Figure 2 b). In other words, the inserted Li is Li^+. The total energies of these systems are less favorable than without Li insertion into the LiPON interior region by 1.16 eV after accounting for the Li metal cohesive energy. Note that V_e assicated with Figure 1 d and Figure 2 b is 0.28 V. The slight difference in V_e compared with that in Figure 1 c is due to the change in the surface dipole moment following the insertion. It is an artifact of our finite simulation cell. Although V_e is found to be slightly too high to correspond to the true 0.0 V vs. Li^+/Li(s), we can at least conclude that at $V_e \approx 0.12$–0.28 V, long range electron transfer into the interior of our LiPON model should not occur.

LiPON chain or fragment on Li(s) surface

The previous section fails to explain why LiPON decomposes on Li metal surfaces at room temperature.[15] Next we consider the fact that LiPON is not crystalline. It consists of short chains in disordered environments.[55] We attempt to model such regions as a single Li_2PO_2N chain deposited on Li metal. Figure 3 a is obtained by removing all other periodically replicated chains in Figure 1 a, and re-optimizing the atomic configuration. This lifts structural constraints (e.g., hindrance of local rotation along the P–N–P chain) that stabilize LiPON against bond breaking.

There are 12 P–N bonds in the LiPON backbone in the simulation cell, 6 P–O bonds with O atoms in contact with the metal surface, and another 6 P–O bonds with O atoms pointing outwards (Figure 3 a). Figure 3 b depicts a configuration where one of the first group of P–O bonds is broken. The reaction results in $\Delta E = -1.15$ eV. The products are more exothermic than those obtained by breaking P–O bonds in the crystalline LiPON slab (Figure 1 b). Our attempt to compute a reaction barrier for this reaction leads to breaking a P–N bond in addition to the initial P–O cleavage event (Figure 3 c), yielding a very exothermic $\Delta E = -2.41$ eV relative to the initial intact LiPON chain. This suggests that breaking P–N bonds in a LiPON chain exhibits lower barriers than breaking P–O, and that P–O cleavage intermediates are unlikely to be the first reaction products.

Next we focus on the twelve P–N bonds. Figure 3 d depicts the optimzed configuration after breaking one of these bonds. ΔE is −2.04 eV. The reaction is highly exothermic, in contrast to the analogous reaction in the slab geometry discussed in the last section. The terminal N atom generated by the broken bond "burrows" into the Li metal region, becoming coordinated to 4 Li atoms (Figure 3 d). The LiPON chain undergoes significant conformational changes to accommodate this motion. Such motions are hindered in a LiPON crystal environment (Figure 1 a).

However, $\Delta E^* = 1.63$ eV is predicted. It is smaller than ΔE^* for P–O bond cleavage, as described in the last section, but remains too large for a room-temperature, one-hour reaction timescale. At the transition state, the P–N distance is 2.21 Å. Incidentally, the combination of large negative ΔE and large positive ΔE^* is not exceptional. This is one of many examples where a large "thermodynamic driving force" is correlated with a slow reaction rate. It shows that ΔE and ΔE^* are not necessarily correlated, and that reaction barriers must be explicitly computed to understand interfacial reactions.

We have also attempted to break the other eleven P–N bonds, one by one. Two attempts revert back to the intact LiPON chain structure. The other nine yield exothermic reactions. The ΔE values of the resulting metastable structures vary from −0.87 to −1.32 eV, depending on whether the N atom broken off from the phosphorus is 4- (Figure 3 d), 2- (Figure 3 e), or 3-coordinated (Figure 3 f). They average to $\Delta E = -1.20 \pm 0.10$ eV. Given the low barriers associated with Li motion on its metal surfaces, subsequent atomic configuration rearrangement from the less exothermic (ca. −0.87 eV) to very exothermic (ca. −1.63 eV) metastable product configurations through Li diffusion on the metal surface may occur readily, but this is not the object of our studies. Instead, we focus on the barrier associated with primary P–N bond cleavage, which should be the rate-limiting step. We have computed the reaction barriers of four of the ten P–N cleavage reactions, in addition to the ΔE^* values associated with $\Delta E = -1.63$ eV. They average to $\Delta E^* = 1.54 \pm 0.15$ eV. The barriers are too high to permit room-temperature reactions at reasonable timescales.

Experimentally, LiPON is known to be composed of finite chains. In Section S3 of the Supporting Information, we consider short LiPON fragments instead of infinite chains. Those cal-

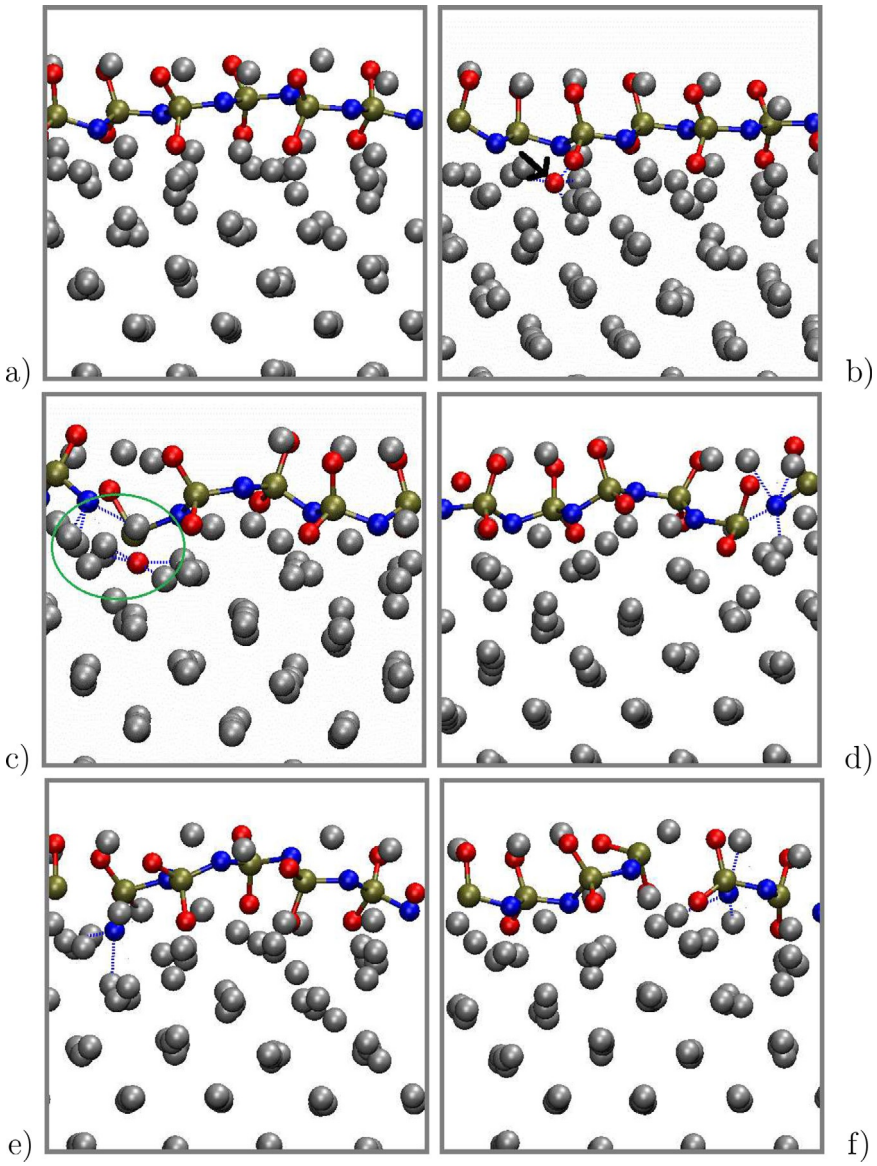

Figure 3. Simulation cell with LiPON chain on Li metal. :a) intact; b) broken P–O bond; c) attempting to calculate barrier to (b) breaks a P–N bond instead; d–f) broken P–N bond with edge N atom coordinated to 4, 2, and 3 Li atoms, respectively. For color scheme, see Figure 1.

culations suggest that the terminal P–O and P–N groups of LiPON fragments, bonded to 4-coordinated P^{5+} atoms, are about as kinetically stable as interior bonds.

Effects of anode voltage on LiPON chain

The instantaneous electronic V_e for the reactant configuration in Figure 3a is predicted to be 0.57 V. At this potential, Li metal should dissolve into the electrolyte as Li^+, releasing e^-. In other words, the calculations associated with Figure 3 are not at electrochemical equilibrium,[28] but reflect a computational overpotential of $\Phi = 0.57$ V. To lower the voltage to the equilibrium value of 0 V, we expand the *x*-lattice constant from 16.41 Å to 23.06 Å. The simulation cell is created by taking the adsorbed LiPON geometry in Figure 3a and adding a strip of bare Li(001) slab. Therefore the LiPON adsorption geometry should be unchanged. Next, we add 4 $[(CH_3)_2O]_2Li^+$ units adsorbed on the Li(001) surface away from the LiPON chain (Figure 4a,b). Ether $[(CH_3)_2O]$ molecules are chosen because they are kinetically stable against lithium metal and do not decompose during optimization calculations. In the charge-neutral simulation cell, the positive charges of the 4 added, ether-coordinated Li^+ induce negative surface charges on the Li metal surface. This results in a surface dipole density that reduces V_e to 0.04 V.[28] On this surface, breaking one of the P–N bonds (Figure 4b) now yields $\Delta E = -1.59$ eV and $\Delta E^* = 1.61$ eV.

Figure 3d, associated with breaking the same bond at $V_e =$ 0.57 V in a smaller simulation cell, have −2.04 eV and 1.63 eV for these values. Despite the decrease of V_e, which can be expected to increase the exothermicity of an electrochemical reaction, ΔE does not become more negative. The smaller $|\Delta E|$ magnitude for Figure 4b compared with Figure 3b may arise from subtle reorientation of the $[(CH_3)_2O]_2Li^+$ units. ΔE^* is almost unchanged. This voltage independence suggests that

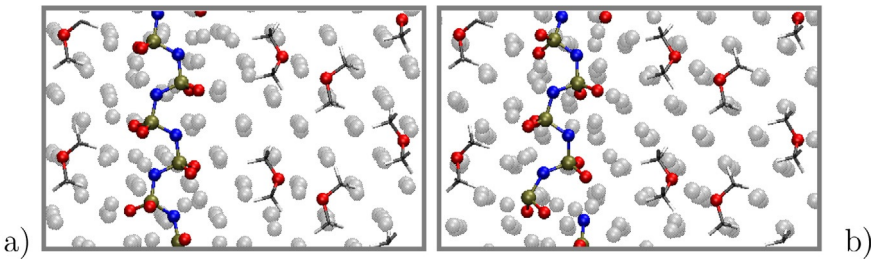

Figure 4. Intact (a) and decomposed (b) LiPON chain on enlarged Li(100) surface simulation cell with 4 $[(CH_3)_2O]_2Li^+$ units, which lower the voltage. The LiPON configurations are similar to those in Figure 3 c,d. For color scheme, see Figure 1.

the rate-determining step of the reaction "does not involve" e^- transfer from the Li electrode. This conclusion is surprising. Many charge transfer reactions, like water reduction or oxidation on metal surfaces, exhibit ΔE values that vary linearly with the overpotential Φ. In DFT calculations, the voltage dependence is often added a posteriori to DFT values as ($ne\Phi$), where n is the number of electrons transferred per reaction and e is the electronic charge.[68] Regarding ΔE^*, the Butler–Volmer equation assumes modification of the reaction barrier by $n\alpha e\Phi$, where α is typically 0.5.[67]

The fact that neither ΔE nor ΔE^* becomes more negative with decreasing Φ suggests that the bond-breaking in LiPON on lithium metal is a surface chemical, not electrochemical, reaction. In metal surface catalyzed electrochemical reactions,[68] the electrons transferred to the solution induce a delocalized surface charges on the metal electrode. In the reaction between Li(100) and the LiPON chain, we propose that two Li atoms on the metal surface turn into discrete Li^+, with their electrons donated to the LiPON chain and no delocalized positive charge induced on the electrode surface. In this way, the values of V_e associated with Figures 3 and 4 do not affect the reaction energetics. Note that it is difficult to quantify the charge distribution on lithium metal surfaces. Bader charge decomposition yields ambiguous, nonuniform charge distributions even on pristine Li(100).

Variations in LiPON backbone

The above calculations have not yet explained the small amount of SEI formation observed upon depositing Li on preformed LiPON.[15] Next we focus on chemical variations along the LiPON chain. LiPON is an amorphous solid with variable chemical compositions.[1] Many experimental papers, as well as some modeling work,[51–53] have shown that some P–O–P linkages exist.

Figure 5 a depicts a P–O–P sequence in the P–N–P chain on the Li surface. It is derived by switching an N and an O atom in Figure 3 a. The total energy of this unreacted chain is 1.56 eV higher than that of Figure 3 a, which has the same stochiometry. This shows that the all-N–P–N backbone model reported by Holzwarth and co-workers[49] is energetically far more favorable, and suggests that P–O–P configurations generated under the fabrication conditions are highly metastable. Figure 5 b represents a configuration where one P–O bond, originally of length 1.65 Å, is broken. For this reaction, $\Delta E = -2.48$ eV and ΔE^* is only 0.90 eV. The other P–O bond in the backbone has an equilibrium bond length of 1.77 Å. Cleaving this bond yields $\Delta E = -3.14$ eV and ΔE^* is only 0.43 eV (Figure 5 c). In both cases, Bader analysis[65] qualitatively indicates that the 3-coordinated P atoms resulting from breaking the bond are in +3 formal charge states. These calculations accomplish our goal of demonstrating the existence of at least one primary reaction that can occur within a one-hour timeframe at room temperature. Fast LiPON reaction with Li metal is also observed in Ref. [53], where the model LiPON backbone contains both P–O–P bonds and N-$(P)_3$ motifs, although the anode voltage is not reported there. We have not attempted inserting Li atoms into the "bulk" LiPON region, unlike in Ref. [53]; this approach may be more directly relevant to Li-vapor deposition experimental conditions reported in XPS measurements[15,53] rather than electrochemical interfaces which are the focus of our calculations.

Next, we consider possible reactions subsequent to the formation of the structure in Figure 5 c. Figure 5 d depicts the breaking of a P–N bond where N is not part of the backbone. The reaction is endothermic by 0.72 eV, and should not proceed. Figure 5 e depicts the cleavage of an O-atom from a 3-coordinated P^{3+} atom. This step is exothermic by 0.47 eV. The predicted barrier is lower than those associated with breaking other P–O bonds we have reported earlier, but remains a substantial $\Delta E^* = 1.18$ eV. This magnitude for ΔE^* is consistent with a reaction time scale that is still far beyond 1-hour at room temperature. Finally, Figure 5 f depicts breaking a P–O bond on the N–PO_3 terminus. The reaction is exothermic by 0.28 eV, but the barrier ($\Delta E^* = 1.74$ eV) is again high. This last prediction dovetails with our finding that that 4-coordinated N–PO_3 end groups in short LiPON fragments are kinetically inert at room temperature (see the Supporting Information, Section S3).

From these calculations, we conclude that LiPON can react with Li metal in a one-hour time frame at room temperature, by cleaving P–O bonds within metastable P–O–P sequences in the backbone. After the initial bond breaking, the undercoordinated P^{3+} atom is slightly more reactive; subsequent P^{3+}–O bond breaking exhibits lower barriers than P^{+5}–O or P^{+5}–N linkages, but the reaction rates associated with such reactions remain low compared to battery operation timescales. Surprisingly, despite the thermodynamic instability of LiPON against lithium,[56] LiPON without P–O–P or $N(P)_3$ in the backbone is kinetically robust on Li surfaces. In contrast, C–O bonds at

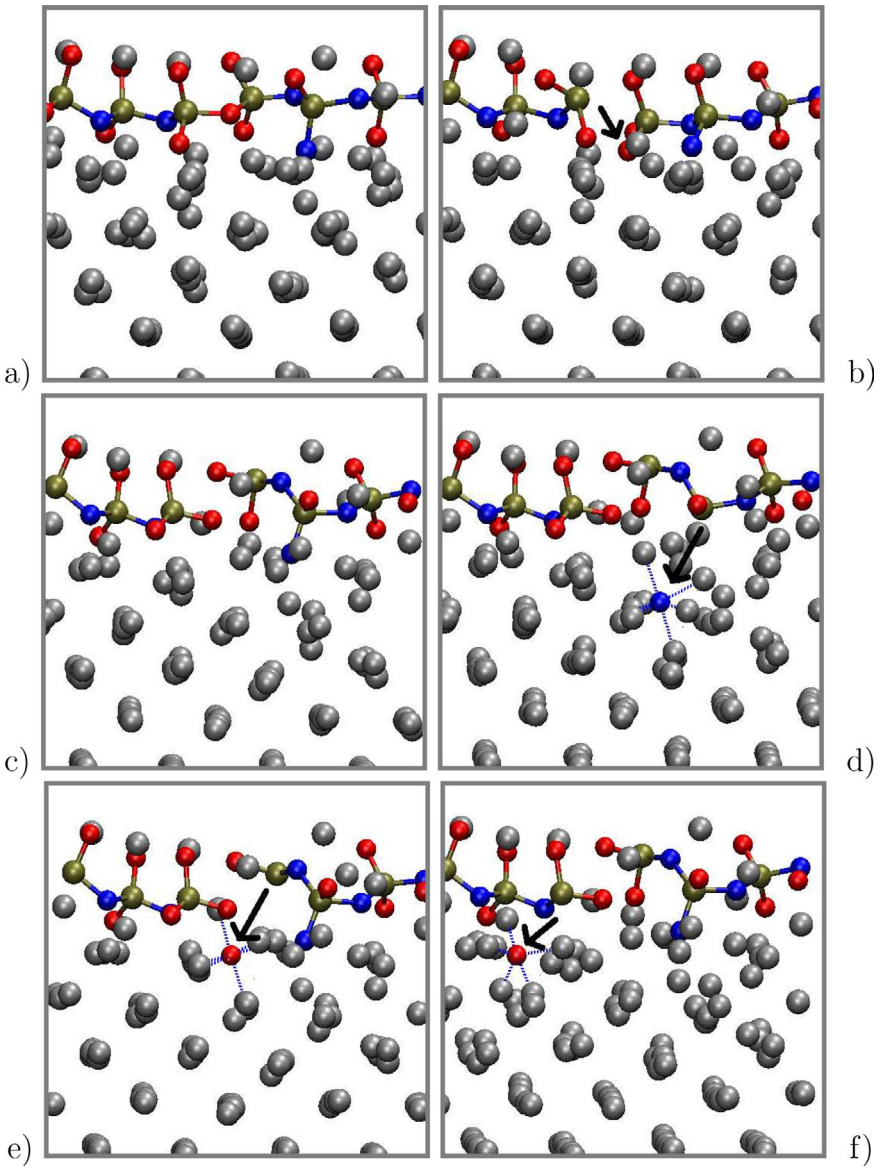

Figure 5. a) LiPON chain with one P–O–P linkage on Li metad. b) Broken P–O bond along the backbone. c) A different broken P–O bond along the backbone. d) Breaking a P–N bond in (c). e, f) breaking two different P–O bonds in (c). For color scheme, see Figure 1.

Li_2CO_3/Li(s) interfaces exhibit far lower ΔE^* values, likely because the C atoms there are only 3-coordinated and have empty p orbitals.

LiPON/Li_xCoO_2(104) interfaces

Explicit interface

This section focuses on the interface between model LiPON and Li_xCoO_2(104) (Figure 6a). The predictions herein are more qualitative, partly because of uncertainties in the voltages associated with the simulation cells.

Small values of x in Li_xCoO_2 are consistent with high equilibrium voltage, which should increase degradation.[9] In this study, x is set to a fairly large value, 0.83, to facilitate convergence of DFT calculations (see the Technical Section and Section S1 in the Supporting Information for details). The cobalt spin states are also depicted in Figure 6. Cobalt adopts low-spin Co^{3+} and low-spin Co^{4+} states in the interior of the cathode slab. Half of the cobalt ions at the interface are bonded to LiPON O atoms; they are 6-coordinated low-spin Co^{3+}. In contrast, 5-coordinated cobalt ions at the surface are in intermediate-spin Co^{3+}[23,47] and high-spin Co^{4+} states. There are a total of 63 net up-spins in these simulation cells. Switching to 65 net unpaired electrons changes ΔE^* by only 0.025 eV.

Figure 6a–d depicts the configurations before and after moving an O atom from the Li_xCoO_2 (LCO) surface to a LiPON N atom at the interface. The N–O distances in these configurations are 2.36 and 1.35 Å, respectively. The distance between the N atom and one of the two P atoms to which it is bonded

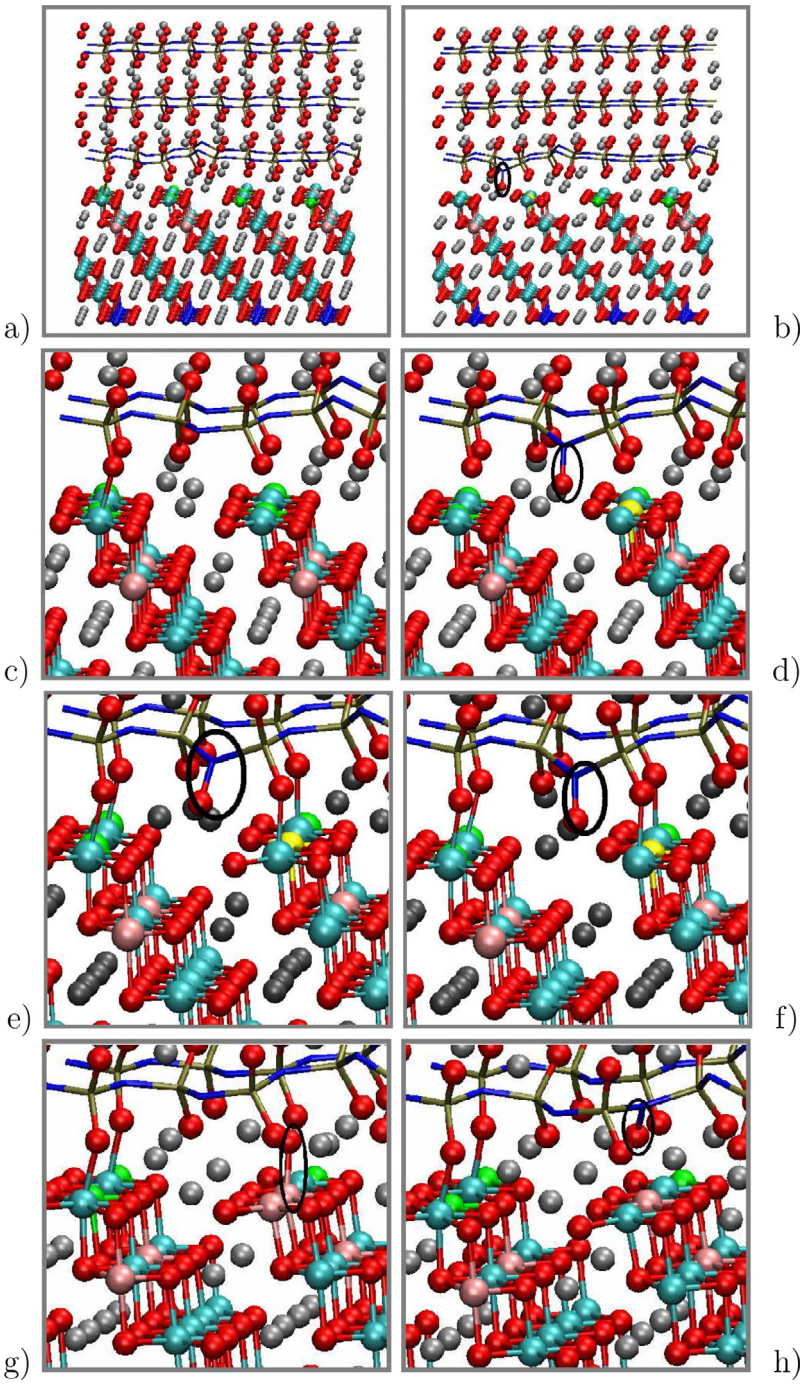

Figure 6. a, b) Original and reacted LiPON slab on Li_xCoO_2(104) surface. Circle indicates the formation of a N–O bond. c, d) Same as (a) and (b), respectively, in expanded views. e, f) Similar to (d), but with distinct Li^+ removed from the reaction zone. g, h) Similar to (c) and (d), respectively, but with an extra Li_2O unit added to the interface. Low and high spin Co^{4+} are depicted as pink and green spheres, respectively. Low, intermediate, and high spin Co^{3+} are depicted as cyan, blue, and yellow spheres, respectively. The rest of the color scheme is as in Figure 1, but P and N atoms are now depicted as sticks, rather than spheres.

increases from about 1.65 Å to 1.75 Å. The 5-coordinated Co^{4+} on the surface originally bonded to the transferring O^{4-} (Figure 6c, green) has turned into a 4-coordinated Co^{3+} (Figure 6d, yellow). It now has four unpaired electrons, reminiscent of 4-coordinated Co^{3+} on the stoichiometric (110) surface.[47] Another low-spin 6-coordinated Co^{4+} in the second oxide layer has become a low-spin Co^{3+}. These changes are consistent with the loss of two e^- from the transferring O^{2-} to LCO. In other words, LiPON has been oxidized. As further confirmation, maximally localized Wannier orbital analysis shows that, in the P–(NO)–P group created, a charge-neutral O atom is transferred, forming a dative covalent bond with the N atom. In contrast, oxygen atoms on the unreacted cathode surface have formal charges of −2. ΔE and ΔE^* for this reaction are

+0.29 eV and +1.09 eV, respectively. This indicates that the O-transfer reaction is thermodynamically unfavorable and kinetically slow.

Increasing the cathode voltage should favor oxidation of LiPON. Rigorously speaking, raising the voltage (V_e) requires lowering the cathode Fermi level. This should be accompanied by removal of Li^+ and e^- pairs in a consistent, grand canonical ensemble manner; Li atoms with vacancy formation energies below $|e|V_e$ plus the metal cohesive energy per Li atom should be removed from the simulation cell. As Li_xCoO_2 is a polaronic conductor with no band gap in parts of the phase diagram, the simplest way to model voltage dependence is to add a metallic "current collector".[28] However, in our case, net spin can accumulate in the metal slab, which would hinder control of the total spin in LCO. Determining which Li atom(s) to remove in the interfacial region is also a difficult task, given the disordered configuration there; removal of many distinct interfacial Li atoms must be attempted. Here we make a local approximation. We remove one Li^+ plus e^- from the system, and recompute ΔE and ΔE^*. Rigorous voltage determinations[28] are deferred to future work.

Figure 6e and f are obtained by removing one Li from Figure 6d. They represent two Li deletion choices, and have three Li atoms in the reaction zone instead of four Li, as in Figure 6d. The pre-reaction configurations are similar to Figure 6a and are not shown; compared with Figure 6c, they both entail an energy cost of 4.30 eV after accounting for the chemical potential of the Li removed. Although not rigorous, this suggests that the "voltage" associated with Li loss is about 4.30 V vs. Li^+/Li(s) in both cases before O transfer, if the Li content is indeed at equilibrium with the instantaneous V_e. ΔE values associated with O transfer from the LCO surface to LiPON are predicted to be +0.11 and +0.10 eV, whereas ΔE^* values are also almost indistinguishable (0.98 eV and 0.95 eV).

In general, $\Delta E < 0$ is required for reactions to proceed. However, further lowering the value of x below our current value of $x = 0.83$ is expected to be consistent with a more negative, ultimately favorable ΔE. Section S4 of the Supporting Information further suggests that the DFT+U method used in this work overestimates ΔE; a more generally accurate functional like PBE0 should reduce ΔE and render the reaction exothermic. Finally, in Section S5 of the Supporting Information, we show that a similar O-transfer reaction between this crystalline LiPON model and the Li_xCoO_2(110) surface is exothermic by 0.36 eV, even when using the DFT+U method. Regarding the barrier, ΔE^* values are 0.95 and 0.98 eV in the two panels, consistent with reaction times of roughly one hour at room temperature. Therefore we assert that this set of calculations shows that interfacial reactions between the cathode and the electrolyte are viable at room temperature. These predictions are consistent with apparent oxygen loss from Li_xCoO_2—especially during charging at high temperature.[9,10] The change in spin polarization predicted at the LiPON/Li_xCoO_2 interface may be measurable. Note that our calculations pertain to high equilibrium voltages, not as-grown conditions.

Section S4 of the Supporting Information demonstrates that moving an O atom from the bulk (as opposed to the surface) of LCO to LiPON is energetically more unfavorable. This trend is generally observed on cathode oxide surfaces.[69] Hence continuous loss of O atoms from LCO must be mediated by other mechanisms. One possibility is the migration of undercoordinated surface Co from their surface sites, which creates more undercoordinated oxygen at LCO surfaces.

So far we have focused on flat Li_xCoO_2(104) surfaces. Other models, in which (104) surfaces are covered with CoOH groups, owing to reaction with H_2O in the atmosphere, have been proposed.[70] This possibility is explored in Figure 6g and h by adding a Li_2O formula unit at the interface, with the added O^{2-} attached to a formerly 5-coordinated Co ion. By using computational procedures similar to those described above, we find that $\Delta E = -1.61$ eV and $\Delta E^* = 0.10$ eV for transferring the newly added O atom from the Co ion to a LiPON nitrogen atom nearby. The reaction proceeds much more readily since there is no need to create an oxygen vacancy on the cathode surface. This calculation strongly suggests that no Co–O bond with the O atom sticking out of the surface survives contact with LiPON.

Excess oxygen diffusion inside LiPON

Next we consider possible subsequent oxygen migration steps. Here we turn to LiPON bulk "crystal" models not in contact with Li_xCoO_2 to represent interior LiPON regions away from the interface. This is done to reduce the computational cost. Figure 7a depicts a LiPON crystal supercell with eight formula units and one O atom added to one of the LiPON N atoms, as in Figure 6d. Figure 7b depicts another optimized configuration where the added O atom has been manually moved to an equivalent position on a neighboring LiPON chain. The two configurations have identical energies. The diffusion barrier be-

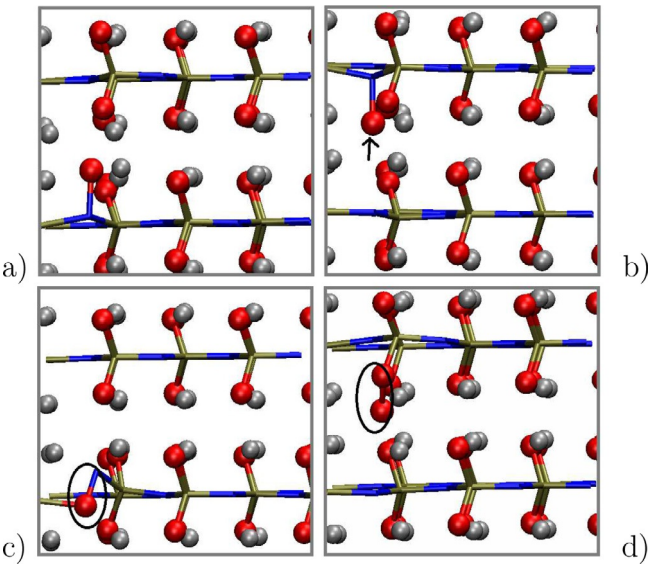

Figure 7. Li_2PO_2N bulk crystal simulation cell with eight formula units and one extra O atom bonded to a N atom in the backbone. a) and b) are two topologically equivalent configurations with N–O bonds and have equal energies. The text describes the transfer of the extra O atom between them. c) O atom inserted between P and N. d) O atom added to a LiPON O atom.

tween them is a low 0.68 eV. This suggests that O atoms abstracted from Li_xCoO_2 readily diffuse inside LiPON once it is away from the interface, possibly aiding further creation of oxygen vacancies on the cathode surface.

We also explore other locations where an additional O atom can insert into LiPON. Figure 7c depicts a P–O–N motif which is 0.17 eV more favorable than the P–N–O linkage in Figure 7a,b. This configuration can be a reaction product or intermediate subsequent to N–O bond formation in Figure 7a and b. In contrast, O–O bond formation (Figure 7d) is less favorable than Figure 7a and b by 0.64 eV. N–O bond formation appears a crucial step in LiPON oxidation by LCO. We predict that N atoms are the reactive sites at LiPON/cathode interfaces and propose that a lower N content at the interface may provide better kinetic LiPON stability against Li_xCoO_2.

Although various defects have been considered in LiPON simulations,[71] to our knowledge there has been little effort to model or measure the migration of excess oxygen bonded to N atoms in the LiPON backbone. It is possible that the amorphous arrangements of LiPON chains in experimental samples may impede interchain oxygen transport.

Conductivity and XPS

This section reports some conductivity and XPS measurements relevant to the LCO/LiPON interface calculations above. Experimental LiPON is amorphous, unlike the crystalline models. However, the local structures responsible for chemical reactions are not expected to depend on LiPON long-range order.

The electronic conductivity of $LiCoO_2$ varies by as much as six orders of magnitude, depending on the Li concentration,[72–74] and can be used as a sensitive probe of lithitation.[74] To experimentally investigate the transfer of Li between $LiCoO_2$ and a LiPON electrolyte, electrochemical transistors were fabricated consisting of a thin film stack of sputtered $LiCoO_2$/LiPON/$LiCoO_2$ layers, with the bottom $LiCoO_2$ acting as a transistor channel and the top $LiCoO_2$ acting as an electrochemical gate. Sputtered LiPON is known to yield amorphous LiPON.[6] The fully fabricated transistor cell consists of 100 nm of high-temperature (HT) $LiCoO_2$, 400 nm of LiPON, 100 nm of low-temperature (LT) $LiCoO_2$. The transistor channel was fabricated using photo lithographically defined Pt electrodes (60 nm) with channel dimensions of 4 μm length and 1700 μm width. Further details of device fabrication process were described previously.[74]

The electronic conductivity of the bottom $LiCoO_2$ layer was measured after deposition of each subsequent layer to qualitatively understand the Li transfer during sputter fabrication processes. Figure 8 depicts the current vs. voltage characteristics of the transistor source drain terminals with an illustration of the various layers at the time of measurement. The current is measured parallel to the $LiCoO_2$ surface and/or the $LiCoO_2$/LiPON interface. Initially (Figure 8a), there is no external bias normal to the surface. At the same applied voltage parallel to the interface, the current is much higher before LiPON deposition than after (Figure 8a vs. b), indicating that the resistivity has gone up significantly. This is consistent with the transfer of

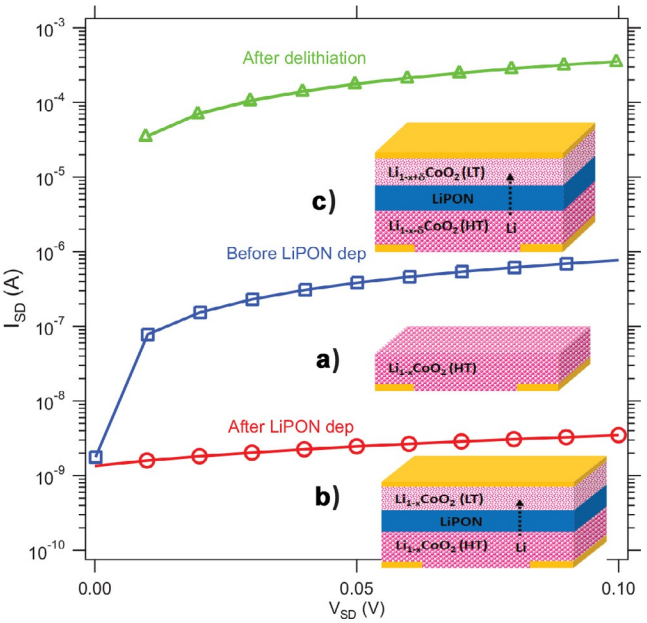

Figure 8. Current (I_{sd}) as a function of applied voltage (V_{ad}) in solid-state devices. Blue: bare $LiCoO_2$; red: $LiCoO_2$ after LiPON deposition; green: same device as depicted in red but with an applied bias that delithiates $LiCoO_2$. (a)–(c), in that order, indicate currents associated with the sequence of events described in the text.

Li (i.e., Li^+ and e^-.) from LiPON to $LiCoO_2$. The latter may be slightly Li-defective when first synthesized. Lithiation of Li_xCoO_2 at $x \approx 1$ is known to increase its resistivity. This point is confirmed by applying an external bias perpendicular to the $LiCoO_2$/LiPON interface, which removes Li from $LiCoO_2$ to the electrochemical gate on the other side of the LiPON film (Figure 8c). The magnitude of the current (green line) goes back up, to a value above that obtained before LiPON deposition.

The results depicted in Figure 8 are consistent with removal of Li^+ and e^- from LiPON. By themselves they do not yield evidence of oxygen migration from $LiCoO_2$ to LiPON. But LiPON oxidation is most readily accomplished by oxidizating either O or N anions. Li^+ and P^{5+} atoms cannot be further oxidized. Adding O atoms to LiPON would be consistent with our predictions in the last section. Note that the excess Li in $LiCoO_2$ could also be the cause of the disorder observed in Refs. [8]–[10]. One possible secondary reaction after the oxygen transfer is a charge-neutral NO molecule release from P–(NO)–P created in the first step, with the LiPON surface losing e^- and Li^+ to Li_xCoO_2 in the processs. This suggestion from our experimental collaboration will be considered in a future computational work.

We have also performed XPS measurements on LiPON deposited on $LiCoO_2$ by atomic layer deposition (ALD) prior to cycling (Figure 9). Our previous studies have shown that this method yields amorphous LiPON in the tested temperature range, as indicated by the lack of identifiable peaks in X-ray diffraction.[33] The Co 2p, O 1s, and N 1s spectra were obtained after 0, 6, 30, and 100 cycles of ALD Li_2PO_2N grown at $T=$ 250 °C, resulting in nominally 0, 3.6, 18, and 60 Å of coverage over LCO, respectively. The deposition process immediately

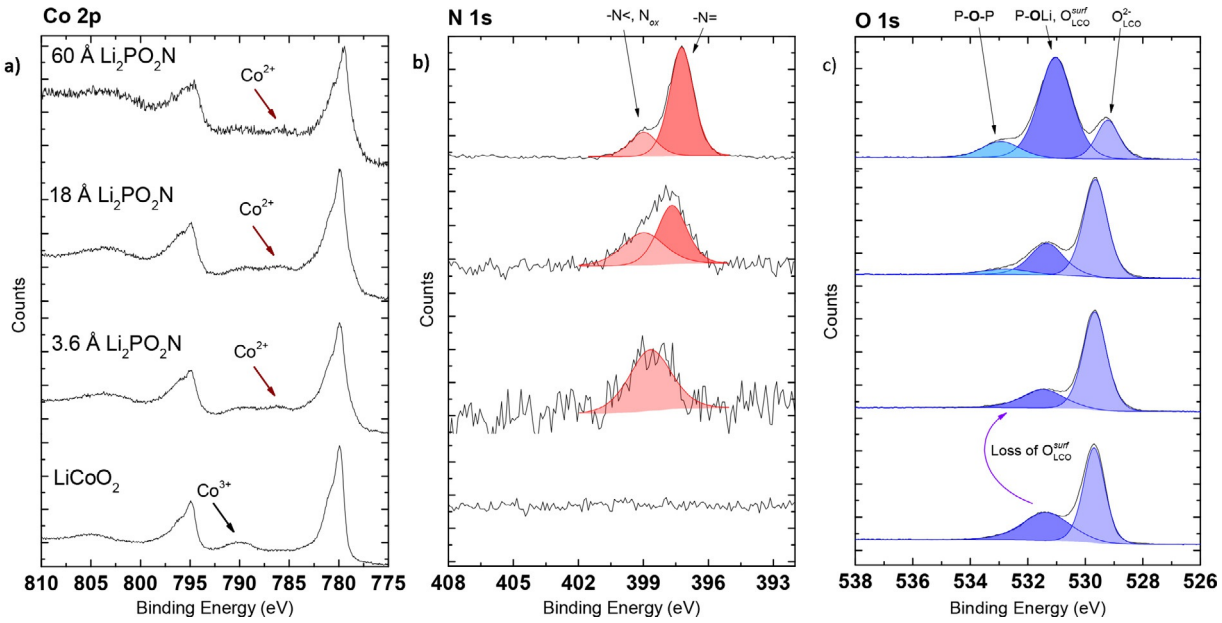

Figure 9. XPS spectra for various thicknesses of LiPON films deposited on $LiCoO_2$: a) Co; b) N; c) O.

produces a satellite feature in the Co 2p spectrum consistent with reduction of surface states to Co^{2+}. The O 1s spectrum shows a loss in what is often considered "surface" or "undercoordinated" O feature in Li_xCoO_2, though this is not a strong definition. It could be consistent with loss of these oxygen atoms to the ALD precursors/Li_2PO_2N layer, as the N 1s spectrum clearly shows that the N atoms closest to the interface are all in a more highly oxidized state than in the "bulk" Li_2PO_2N. This is similar to what other groups have reported for other methods of growing LiPON.[13,17] The N–O bond formation predicted in Figure 6 is consistent with oxidized nitrogen. There is a clear signature of the P–O–P sequence in the O spectra. This feature is reflected in our anode model depicted in Figure 5.

Note that some of these features, especially Co^{2+}, are at least partially produced by vacuum annealing of LCO at 250 °C. Co^{2+} is not seen in our calculations because the partial delithiation in our DFT models should yield Co^{3+} and Co^{4+}. We also stress that the samples and devices analyzed in Figure 9 are distinct from those described in Figure 8.

Discussion and Comparison with Experimental Data

Our interfacial simulations focus on initial reaction barriers in crystalline models. They are not meant to predict final chemical speciations. Hence comparisons with structural measurements require some extrapolation—especially since experimental LiPON is amorphous. The previous section has revealed qualitative agreement between our predictions and measurements. This section focuses on comparison with published experimental work.

As stated in the Introduction, all-solid-state batteries with Li metal anode, $LiCoO_2$ cathode, and LiPON electrolytes have been shown to cycle well if the LiPON film is sufficiently thick, especially at room temperature.[5,9,10,33] At the same time, some degradation products and/or disordered regions are reported at both cathode[9,10,13,17] and anode[15,53] interfaces. Although the specific LiPON structure or composition used in experiments may not coincide with our models or even with each other, our predictions can help interpret these results.

At the anode interface, we predict that only P–O–P sequences can readily break at ambient conditions. This mechanism is also proposed in Ref. [15] (see in particular Figure 4 of that report). Most other bond-breaking barriers, such as those involving P–N cleavage, are predicted to exhibit $\Delta E^* > 1.5$ eV. This suggests that temperatures of >450 K, which approach the Li melting point, are needed to make these P–N–P/Li(s) reactions fast enough to occur at room temperature. This finding is consistent with the survival of LiPON XPS signals seen in vapor deposition of Li on LiPON.[15,53] The ratio between triply and doubly coordinated N atoms in amorphous LiPON significanty decreases upon deposition Li,[15] consistent with the hypothesis that triply-coordinated N, which does not exist in our model, is far more reactive than doubly-coordinated N. To our knowledge, the Li/LiPON interface has not been reported as a major source of degradation in all-solid-state batteries. Our predictions are also consistent with the kinetic stability observed in Pt/LiPON/Li devices, which are stable for months with little change in conductivity,[33] although some SEI products from ALD-deposited LiPON likely also help passivation.

At the cathode surface, a 10 Å thick NO_2^- and/or NO_3^- layer has been estimated from XPS measurements.[13,17] The formation of N–O bonds is consistent with the first step reaction mechanism predicted in our calculations (Figure 6).

More recently, disordered $LiCoO_2$ regions in contact with LiPON have been reported in STEM studies.[9,10] The disordered layer can be hundreds of nanometers thick at room tempera-

ture prior to cycling. Its thickness increases with charge–discharge and especially with temperature. However, the all-solid-state battery retains its capacity after 250 cycles.[9] The LiPON region does not exhibit significant changes, possibly because LiPON is already amorphous. Co_3O_4 and Li_2O_2 are identified in the disordered Li_xCoO_2 region by STEM and electron energy loss spectroscopy (EELS).[9,10] These measurements suggest the presence of Co^{2+} at the interface and imply loss of oxygen from Li_xCoO_2. Oxygen transfer from $LiCoO_2$ to LiPON are proposed to occur already at the as-grown, uncycled $LiCoO_2$/LiPON interface in these experimental works. Peroxides species are also reported at these interfaces.[8] Recall that our XPS measurements (Figure 9) also indicate the presence of Co^{2+}.

Our calculations focus on charged Li_xCoO_2 with $x=0.83$, which only contains Co^{3+} and Co^{4+} ions. No Co^{2+} is expected at this value of x. We predict loss of oxygen from Li_xCoO_2. Upon transfer of an O atom to LiPON, two Co^{4+} ions turn into Co^{3+}. The oxygen vacancies formed may be consistent with a disordered Li_xCoO_2 region.[8] Our calculations focus on the initial stages of reaction, and provide no information about the thickness of the reacted cathode layer. We do not observe peroxide formation. Peroxide-like structures have been predicted in oxygen-depleted Li_2MnO_3.[75] In our simulation cells, however, N–O bond formation is found to be more favorable than O–O.

Conclusions

We have applied electronic structure DFT calculations to study interfacial degradation reactions between model crystalline Li_2PO_2N and the surfaces of two electrodes: Li metal and Li_xCoO_2. Some experimental corroboration is also provided; this assumes that interfacial reactions on amorphous and crystalline LiPON models are similar. The predictions are relevant to the interfacial film ("solid–electrolyte interphase" or "SEI") products formed during cycling of all-solid-state batteries using LiPON solid electrolytes. LiPON proves to be an interesting case study. Single-phase thermodynamics calculations predict instabilities at both interfaces, which do not distinguish the extent of reactions formed in the two cases. Herein we have instead focused on models with explicit interfaces and calculated the reaction activation energies. Multiple reaction sites and bond-breaking events are considered. The predictions suggest that most initial reactions on the anode surface are slow for LiPON with P–N–P backbone and atomic layer deposition (ALD)-like stoichiometry[33], whereas cathode interfacial reactions can occur within battery cycling timescales.

On Li(001) surfaces, ordered LiPON chains with P–N–P backbones, P–O side groups, and 2-coordinated N atoms are found to exhibit P–N and P–O cleavage barriers in excess of 1.4 eV, which correspond to reactant half lives far in excess of battery operation timescales. In contrast, P–O–P sequences, which are much less energetically favorable but known to exist in LiPON, are found to exhibit faster bond-breaking reactions. However, subsequent reactions again exhibit barriers exceeding 1 eV and are slow. The electrode potential does not strongly affect the exothermicity or the reaction barrier. From these calculations, some SEI products are expected at this interface, but extensive degradation is not expected at room temperature. This is consistent with experimental data showing that some 2-coordinated N atoms persist after lithium vapor deposition[15]. Our model thus helps pinpoint less-reactive LiPON motifs. Our predicted reaction rates are much lower than those in models with both $N(P)_3$ and P–O–P groups[53].

At LiPON/Li_xCoO_2(104) interfaces, cobalt ions can exhibit five different spin/charge states, which makes reproducible calculations of Kohn–Sham wavefunctions difficult. We believe this is a general phenomenon associated with Li_xCoO_2 surfaces, and propose that extra care should be taken in future modeling of interfacial spin states associated with this material. By working close to $x=1$ and propagating wavefunctions quasi-continuously from product to reactant, estimates for reaction barriers are obtained. We find that even the surfaces of chemically ordered, crystalline LiPON slabs are oxidized by Li_xCoO_2 within battery cycling (one-hour) timescale at room temperature. The LiPON N atom abstracts an O atom from the oxide surface in the process. O atoms added to crystalline LiPON interior are mobile, potentially creating pathways for further degradation of Li_xCoO_2 as battery cycling continues. We propose that interfaces with less nitrogen content may yield less degradation on cathodes.

This work emphasizes kinetics, not thermodynamics, at solid–solid interfaces. Under processing (ca. 200 °C) and cycling (room temperature) conditions, electrode/electrolyte interfaces may not be at thermodynamic equilibrium and metastable starting materials and/or intermediate products may persist. In addition to shedding light on reaction kinetics, our calculations elucidate the low-barrier initial bond-breaking steps involved in degradation reactions. This will facilitate future design of solid-state materials and interfaces more resilient to degradation.

Technical Section

DFT calculations are conducted by using the Vienna Atomic Simulation Package (VASP) version 5.3[76–78] and the PBE functional.[79] Modeling Li_xCoO_2 with $x\approx1$ requires spin-polarized DFT+U augmented treatment[80] of Co 3d orbitals. The U and J values depend on the orbital projection scheme and DFT+U implementation details; here $U-J=3.30$ eV is adopted, in accordance with the reported values.[46] In Section S4 of the Supporting Information, the more computationally costly PBE0 functional,[81] which is generally more accurate, is used for spot-checks.

We adopt one of the crystalline LiPON (Li_2PO_2N "s2") crystal structures created by the Holzwarth group.[49] This model consists of parallel zig-zag LiPON chains, and is chosen because the lattice dimensions, re-optimized using the PBE functional, best match the Li(001) supercell size.

Our interfacial model systems are charge-neutral asymmetric slabs. The details of representative simulation cells are listed in Table 1. The standard dipole correction is applied to negate image interactions in the periodically replicated, charge-neutral anode-side simulation cells.[82] This correction is found to be 0(1) meV on the cathode side and is omitted therein.

Table 1. Computational details of representative simulation cells. LiPONs, LiPONc, and LiPONf refer to a LiPON slab, a single chain, and a fragment, respectively. Typically the configurations are first optimized using Γ-point sampling and then re-optimized using the listed *k*-point grid.

System	Dimensions	Stoichiometry	*k*-sampling	Figure
Li(s)/LiPONc	14.28×16.41×28.00	$Li_{172}P_6O_{12}N_6$	2×2×1	3a
Li(s)/LiPONf	14.28×23.06×28.00	$Li_{236}P_6O_{12}N_6$	2×1×1	S1a
Li(s)/LiPONs	14.28×16.41×40.00	$Li_{274}P_{54}O_{108}N_{54}$	2×2×1	1a
LCO/LiPONs	11.41×23.62×36.00	$Li_{195}Co_{96}O_{312}P_{60}N_{60}$	2×1×1	6a
LiPON	10.94×9.26×9.52	$Li_{32}P_{16}O_{32}N_{16}$	2×2×2	7a
$Li_xCoO_{2-\delta}$	8.53×8.53×14.18(hex)	$Li_{25}P_{27}O_{53}$	2×2×1	NA

Reaction barriers are computed by using the climbing-image nudged elastic band (cNEB) method.[83] The barriers associated with LiPON P–N bond cleavage on lithium surfaces are nontrivial to compute because cNEB can mistake (P–O)–Li^+ dissociation with true bond-breaking events. When the cNEB approach yields a configuration close to the barrier top, we typically switch to quasi-Newton algorithm optimization of that single configuration until the maximal force on each atom is less than 0.07 eV Å^{-1}. When Li_xCoO_2 slabs are present in the simulation cell, we have propagated wavefunctions quasi-continuously from product to reactant. More details on computational and experimental methods are found in Section S1 of the Supporting Information.

Lithium is a metallic conductor and its Fermi level (E_F) is well defined. Work functions are computed as differences between E_F and vacuum levels. The work function minus 1.37 V is the instantaneous electronic voltage (V_e) relative to Li^+/Li(s). We distinguish V_e from the equilibrium or ionic voltage, which is a function of the lithium chemical potential referenced to lithium metal cohesive energy.[28] There is no reason to expect that DFT interfacial models are automatically at electrochemical equilibrium, in the sense that the two definitions are equal. As discussed in the text, such models are more likely to be at overpotential conditions unless care is taken.

The charge states of Co ions are determined by cross-referencing maximally localized Wannier function analysis[84] and approximate local spin polarizations s_z predicted by the VASP code. $|s_z| \approx 0.0$, 1.0, 2.0, 2.2, and 2.8 are assigned to low-spin Co^{3+}, low-spin Co^{4+}, intermediate-spin Co^{3+}, high-spin Co^{4+}, and high-spin Co^{3+}, respectively. Note that the VASP code requires that Wannier calculations be conducted by using Γ-point Brillouin zone sampling.

Acknowledgements

We thank Yue Qi for useful discussions. This work was performed, in part, at the Center for Integrated Nanotechnologies, an Office of Science User Facility operated for the U.S. Department of Energy (DOE) Office of Science. It was supported by Nanostructures for Electrical Energy Storage (NEES), an Energy Frontier Research Center funded by the U.S. Department of Energy, Office of Science, Office of Basic Energy Sciences under Award Number DESC0001160. Sandia National Laboratories is a multimission laboratory managed and operated by National Technology and Engineering Solutions of Sandia, LLC, a wholly owned subsidiary of Honeywell International, Inc., for the U.S. Department of Energys National Nuclear Security Administration under contract DE-NA0003525.

Conflict of interest

The authors declare no conflict of interest.

Keywords: ab initio calculations · batteries · interfaces · LiPON · solid-solid reactions

[1] K. Kerman, A. Luntz, V. Viswanathan, Y.-M. Chiang, Z. Chen, *J. Electrochem. Soc.* **2017**, *164*, A1731.
[2] A. Mauger, M. Armand, C. M. Julien, K. Zaghib, *J. Power Sources* **2017**, *353*, 333.
[3] Y. Ren, K. Chen, R. Chen, T. Liu, Y. Zhang, C.-W. Nan, *J. Am. Ceram. Soc.* **2015**, *98*, 3603.
[4] C. Sun, J. Liu, Y. Gong, D. P. Wilkinson, J. Zhang, *Nano Energy* **2017**, *33*, 363.
[5] J. B. Bates, N. J. Dudney, B. Neudecker, A. Ueda, C. D. Evans, *Solid State Ionics* **2000**, *135*, 33.
[6] J. B. Bates, N. J. Dudney, G. R. Gruzalski, R. A. Zuhr, A. Choudhury, C. F. Luck, J. D. Robertson, *J. Power Sources* **1993**, *43*, 103.
[7] A. C. Luntz, J. Voss, K. Reuter, *J. Phys. Chem. Lett.* **2015**, *6*, 4599.
[8] Z. Wang, D. Santhanagopalan, W. Zhang, F. Wang, H. L. Xin, K. He, J. Li, N. J. Dudney, Y. S. Meng, *Nano Lett.* **2016**, *16*, 3760.
[9] Z. Y. Wang, J. Z. Lee, H. L. L. Xin, L. L. Han, N. Grillon, D. Guy-Bouyssou, E. Bouyssou, M. Proust, Y. S. Meng, *J. Power Sources* **2016**, *324*, 342.
[10] D. Santhanagopalan, D. Qian, T. McGilvray, Z. Wang, F. Wang, F. Camino, J. Graetz, N. J. Dudney, Y. S. Meng, *J. Phys. Chem. Lett.* **2014**, *5*, 298.
[11] Y. Aizawa, K. Yamamoto, T. Sato, H. Murata, R. Yoshida, C. A. J. Fisher, T. Kato, Y. Iriyama, T. Hirayama, *Ultramicroscopy* **2017**, *178*, 20.
[12] K. Yamamoto, Y. Iriyama, T. Asaka, T. Hirayama, H. Fujita, C. A. J. Fisher, K. Nonaka, Y. Sugita, Z. Ogumi, *Angew. Chem. Int. Ed.* **2010**, *49*, 4414; *Angew. Chem.* **2010**, *122*, 4516.
[13] S. Jacke, J. Song, G. Cherkashinin, L. Dimesso, W. Jaegermann, *Ionics* **2010**, *16*, 769.
[14] S. Jacke, J. Song, L. Dimesso, J. Brötz, D. Becker, W. Jaegermann, *J. Power Sources* **2011**, *196*, 6911.
[15] A. Schwöbel, R. Hausbrand, W. Jaegermann, *Solid State Ionics* **2015**, *273*, 51.
[16] R. Hausbrand, G. Cherkashinin, H. Ehrenberg, M. Gröting, K. Albe, C. Hess, W. Jaegermann, *Mater. Sci. Eng. B* **2015**, *192*, 3.
[17] M. Fingerle, R. Buchheit, S. Sicolo, K. Albe, R. Hausbrand, *Chem. Mater.* **2017**, *29*, 7675.
[18] J. Haruyama, K. Sodeyama, Y. Tateyama, *ACS Appl. Mater. Interfaces* **2017**, *9*, 286.
[19] J. Haruyama, K. Sodeyama, L. Han, K. Takada, Y. Tateyama, *Chem. Mater.* **2014**, *26*, 4248.
[20] N. D. Lepley, N. A. W. Holzwarth, *Phys. Rev. B* **2015**, *92*, 214201.
[21] N. D. Lepley, N. A. W. Holzwarth, Y. A. Du, *Phys. Rev. B* **2013**, *88*, 104103.
[22] K. C. Santosh, K. Xiong, R. C. Longo, K. Cho, *J. Power Sources* **2013**, *244*, 136.
[23] M. Sumita, T. Ohno, *Phys. Chem. Chem. Phys.* **2016**, *18*, 4316.
[24] M. Sumita, Y. Tanaka, M. Ikeda, T. Ohno, *J. Phys. Chem. C* **2015**, *119*, 14.
[25] S. S. Chandrasekaran, P. Murugan, *Appl. Surf. Sci.* **2017**, *418*, 17.
[26] K. Thai, E. Lee, *J. Electrochem. Soc.* **2017**, *164*, A594.
[27] J. Song, S. Jacke, G. Cherkashinin, S. Schmid, Q. Dong, R. Hausbrand, W. Jaegermann, *Electrochem. Solid-State Lett.* **2011**, *14*, A189.
[28] K. Leung, A. Leenheer, *J. Phys. Chem. C* **2015**, *119*, 10234.
[29] Operationally, assembling interfaces often involves atomic layer deposition, plasma laser deposition, and other techniques to deposit LiPON or other solid electrolytes on to electrode surfaces. These techniques do not correspond to pressing the flat surfaces of two preformed materials together. Intermixing of electrolye and electrode components at the interface may occur naturally during growth; therefore, the SEI interlayers may result from gas-phase reactions in addition to degradation of fully

formed LiPON. What is needed to address such growth conditions is a comprehensive science of processing conditions.
[30] C. F. Lin, M. Noked, A. C. Kozen, C. Y. Liu, O. Zhao, K. Gregorczyk, L. B. Hu, S. B. Lee, G. W. Rubloff, *ACS Nano* **2016**, *10*, 2693.
[31] C. Gong, D. Ruzmetov, A. Pearse, D. Ma, J. N. Munday, G. Rubloff, A. A. Talin, M. S. Leite, *ACS Appl. Mater. Interfaces* **2015**, *7*, 26007.
[32] V. P. Oleshko, T. Lam, D. Ruzmetov, P. Haney, H. J. Lezec, A. V. Davydov, S. Krylyuk, J. Cumings, A. A. Talin, *Nanoscale* **2014**, *6*, 11756.
[33] A. J. Pearse, T. E. Schmitt, E. J. Fuller, F. El-Gabaly, C.-F. Lin, K. Gerasopoulos, A. C. Kozen, A. A. Talin, G. W. Rubloff, K. E. Gregorczyk, *Chem. Mater.* **2017**, *29*, 3740.
[34] A. C. Kozen, A. J. Pearse, C.-F. Lin, M. Noked, G. W. Rubloff, *Chem. Mater.* **2015**, *27*, 5324.
[35] D. Li, Z. Ma, J. Xu, Y. Li, K. Xie, *Mater. Lett.* **2014**, *134*, 237.
[36] Y. Yoon, C. Park, J. Kim, D. Shin, *Electrochim. Acta* **2013**, *111*, 144.
[37] Y. Kim, G. M. Veith, J. Nanda, R. R. Unocic, M. Chi, N. J. Dudney, *Electrochim. Acta* **2011**, *56*, 6573.
[38] C. S. Nimisha, G. M. Rao, N. Munichandraiah, G. Natarajan, D. C. Cameron, *Solid State Ionics* **2011**, *185*, 47.
[39] Q. Zhang, A. K. Kercher, G. M. Veith, V. Sarbada, A. B. Brady, J. Li, E. A. Stach, R. Hull, K. J. Takeuchi, E. S. Takeuchi, N. J. Dudney, A. C. Marschilok, *J. Electrochem. Soc.* **2017**, *164*, A1503.
[40] P. D. Mani, S. Saraf, V. Singh, M. Real-Robert, A. Vijayakumar, S. J. Duranceau, S. Seal, K. R. Coffey, *Solid State Ionics* **2016**, *287*, 48.
[41] H. Porthault, C. Decaux, *Electrochim. Acta* **2016**, *194*, 330.
[42] S. Tintignac, R. Baddour-Hadjean, J. P. Pereira-Ramos, R. Salot, *Electrochim. Acta* **2014**, *146*, 472.
[43] S. Wenzel, T. Leichtweiss, D. Krüger, J. Sann, J. Janek, *Solid State Ionics* **2015**, *278*, 98.
[44] Y. Iriyama, T. Kako, C. Yada, T. Abe, Z. Ogumi, *Solid State Ionics* **2005**, *176*, 2371.
[45] K. Leung, S. B. Rempe, M. E. Foster, Y. Ma, J. M. M. de Hoz, N. Sai, P. B. Balbuena, *J. Electrochem. Soc.* **2014**, *161*, A213.
[46] D. Kramer, G. Ceder, *Chem. Mater.* **2009**, *21*, 3799.
[47] D. Qian, Y. Hinuma, H. Chen, L.-S. Du, K. J. Carroll, G. Ceder, C. P. Grey, Y. S. Meng, *J. Am. Chem. Soc.* **2012**, *134*, 6096.
[48] L. Giordano, P. Karayaylali, Y. Yu, Y. Katayama, F. Maglia, S. Lux, Y. Shao-Horn, *J. Chem. Phys. Lett.* **2017**, *8*, 3881.
[49] Y. A. Du, N. A. W. Holzwarth, *Phys. Rev. B* **2010**, *81*, 184106.
[50] K. Senevirathne, C. S. Day, M. D. Gross, A. Lachgar, N. A. W. Holzwarth, *Solid State Ionics* **2013**, *233*, 95.
[51] E. Guille, G. Vallverdu, I. Baraille, *J. Chem. Phys.* **2014**, *141*, 244703.
[52] S. Sicolo, K. Albe, *J. Power Sources* **2016**, *331*, 382.
[53] S. Sicolo, M. Fingerle, R. Hausbrand, K. Albe, *J. Power Sources* **2017**, *354*, 124.
[54] S. Xu, G. Luo, R. Jacobs, S. Fang, M. K. Mahanthappa, R. J. Hamers, D. Morgan, *ACS Appl. Mater. Interfaces* **2017**, *9*, 20545.
[55] J. C. Garcia, J. Bareno, J. Yan, G. Chen, A. Hauser, J. R. Croy, H. Iddir, *J. Phys. Chem. C* **2017**, *121*, 8290.
[56] Y. Zhu, X. He, Y. Mo, *ACS Appl. Mater. Interfaces* **2015**, *7*, 23685.
[57] L. Sang, R. T. Haasch, A. A. Gewirth, R. G. Nuzzo, *Chem. Mater.* **2017**, *29*, 3029.
[58] K. Leung, F. Soto, K. Hankins, P. B. Balbuena, K. L. Harrison, *J. Phys. Chem. C* **2016**, *120*, 6302.
[59] K. Leung, *J. Phys. Chem. C* **2012**, *116*, 9852.
[60] K. Leung, *Chem. Mater.* **2017**, *29*, 2550.
[61] K. Letchworth-Weaver, T. A. Arias, *Phys. Rev. B* **2012**, *86*, 075140.
[62] C. D. Taylor, S. A. Wasileski, J.-S. Filhol, M. Neurock, *Phys. Rev. B* **2006**, *73*, 165402.
[63] M. Nielsen, M. Bjorketun, M. H. Hansen, J. Rossmeisl, *Surf. Sci.* **2015**, *631*, 2.
[64] Y. Li, K. Leung, Y. Qi, *Acc. Chem. Res.* **2016**, *49*, 2363.
[65] G. Henkelman, A. Arnaldsson, H. Jónsson, *Comput. Mater. Sci.* **2006**, *36*, 354.
[66] L. Wang, Q. Wang, W. Jia, S. Chen, P. Gao, J. Li, *J. Power Sources* **2017**, *342*, 175.
[67] J. O. M. Bockris, A. K. N. Reddy, M. Gamboa-Aldeco, *Modern Electrochemistry 2A. Fundamentals of Electrodics, 2nd ed.*, Kluwer/Plenum, New York/London, **2000**, p. 1083.
[68] K. Chan, J. K. Norskov, *J. Phys. Chem. Lett.* **2015**, *6*, 2663.
[69] Y. Shin, K. A. Persson, *ACS Appl. Mater. Interfaces* **2016**, *8*, 25595.
[70] J. L. Tebbe, T. F. Fuerst, C. B. Musgrave, *ACS Appl. Mater. Interfaces* **2016**, *8*, 26664.
[71] Y. A. Du, N. A. W. Holzwarth, *Phys. Rev. B* **2008**, *78*, 174301.
[72] M. Ménétrier, I. Saadoune, S. Levasseur, C. Delmas, *J. Mater. Chem.* **1999**, *9*, 1135.
[73] A. Milewska, K. Swierczek, J. Tobola, F. Boudoire, Y. Hu, D. K. Bora, B. S. Mun, A. Braun, J. Molenda, *Solid State Ionics* **2014**, *263*, 110.
[74] E. J. Fuller, F. El Gabaly, F. Leonard, S. Agarwal, S. J. Plimpton, R. B. Jacobs-Gedrim, C. D. James, M. J. Marinella, A. A. Talin, *Adv. Mater.* **2017**, *29*, 1604310.
[75] A. Marusczyk, J. M. Albina, T. Hammerschmidt, R. Drautz, T. Eckl, G. Henkelman, *J. Mater. Chem. A* **2017**, *5*, 15183.
[76] G. Kresse, J. Furthmüller, *Phys. Rev. B* **1996**, *54*, 11169.
[77] G. Kresse, J. Joubert, *Phys. Rev. B* **1999**, *59*, 1758.
[78] J. Paier, M. Marsman, G. Kresse, *J. Chem. Phys.* **2007**, *127*, 024103.
[79] J. P. Perdew, K. Burke, M. Ernzerhof, *Phys. Rev. Lett.* **1996**, *77*, 3865.
[80] S. L. Dudarev, G. A. Botton, S. Y. Savrasov, C. J. Humphreys, A. P. Sutton, *Phys. Rev. B* **1998**, *57*, 1505.
[81] C. Adamo, V. Barone, *J. Chem. Phys.* **1999**, *110*, 6158.
[82] J. Neugebauer, M. Scheffler, *Phys. Rev. B* **1992**, *46*, 16067.
[83] G. Henkelman, B. P. Uberuaga, H. Jonsson, *J. Chem. Phys.* **2000**, *113*, 9901.
[84] N. Marzari, D. Vanderbilt, *Phys. Rev. B* **1997**, *56*, 12847.

Manuscript received: January 4, 2018
Revised manuscript received: March 12, 2018
Version of record online: April 18, 2018